Structural Engineering and Mechanics, *Vol. 59, No. 2 (2016) 291-312*
DOI: http://dx.doi.org/10.12989/sem.2016.59.2.291

Seismic performance evaluation of mid-rise shear walls: experiments and analysis

Y.M. Parulekar*[1], G.R. Reddy[1], R.K. Singh[1], N. Gopalkrishnan[2] and G.V. Ramarao[2]

[1]*Reactor Safety Division, Bhabha Atomic Research Centre, Mumbai, 400085, India*
[2]*Structural Engineering Research Centre, Chennai, 600113, India*

(Received October 8, 2015, Revised April 29, 2016, Accepted May 17, 2016)

Abstract. Seismic performance evaluation of shear wall is essential as it is the major lateral load resisting member of a structure. The ultimate load and ultimate drift of the shear wall are the two most important parameters which need to be assessed experimentally and verified analytically. This paper comprises the results of monotonic tests, quasi-static cyclic tests and shake-table tests carried out on a midrise shear wall. The shear wall considered for the study is 1:5 scaled model of the shear wall of the internal structure of a reactor building. The analytical simulation of these tests is carried out using micro and macro modeling of the shear wall. This paper mainly consists of modification in the hysteretic macro model, developed for RC structural walls by Lestuzzi and Badoux in 2003. This modification is made by considering the stiffness degradation effect observed from the tests carried out and this modified model is then used for nonlinear dynamic analysis of the shear wall. The outcome of the paper gives the variation of the capacity, the failure patterns and the performance levels of the shear walls in all three types of tests. The change in the stiffness and the damping of the wall due to increased damage and cracking when subjected to seismic excitation is also highlighted in the paper.

Keywords: shear walls; shake table tests; quasi-static cyclic tests; analysis; damping

1. Introduction

Nowadays, performance based design approach is gaining importance for assessing structures subjected to earthquake loading. The evaluation of the seismic performance of nuclear power plant structures requires the assessment of shear walls which are its main structural members. In performance based design, the demand on the structures is defined based on the expected level of performances such as immediate occupancy, life safety or collapse prevention as per FEMA-356 (2000). Hence, the realistic evaluation of performances of RC structures subjected to earthquake is the subject of research. The methodology needs to be developed and validated with the experiments for shear walls with different aspect ratios.

Shear walls used in nuclear power plants and other structures like high rise buildings may fail under earthquake due to a variety of mechanisms like flexure, shear, sliding shear or a combination thus resulting in a significant lateral displacement and strength degradation. In high rise buildings,

*Corresponding author, Ph.D., E-mail: yogitap@barc.gov.in

Copyright © 2016 Techno-Press, Ltd.
http://www.techno-press.org/?journal=sem&subpage=8 ISSN: 1225-4568 (Print), 1598-6217 (Online)

a three-dimensional formulation which can be used as a tool in preliminary design is proposed by Carpinteri *et al*. (2012) to analyse the lateral loading distribution of external actions. Earlier, a lot of experiments were carried out on shear walls by many researchers. The response of four squat walls with rectangular or flanged cross-sections under static-cyclic load was examined by Paulay *et al*. (1982). The specimen was designed without strong boundary reinforcement and axial force was not applied on it. It was observed that the failure of the wall was dominated by sliding shear and significant strength loss due to degradation of aggregate interlock. Kassem (2015) gave a closed-form expression for the shear strength of a squat wall that accounts for the contributions provided by the diagonal concrete strut and the web reinforcement. Salonikios *et al*. (2002) carried out an experimental investigation on walls with aspect ratios of 1.0 and 1.5. The wall specimens were reinforced against shear, either conventionally (orthogonal grids of web reinforcement) or with cross-inclined bars. The specimens were tested as cantilevers and those having diagonal reinforcement failed in a predominantly flexural mode, characterized by concrete crushing and reinforcement buckling. Diagonal cracking of the web and sliding at the fixed base were observed for the specimens having no diagonal reinforcement. Similarly Tasnimi (2000) carried out cyclic tests on four mid-rise walls without any axial load. A plastic hinge at the base of the wall was found in all the specimens. It was found that cyclic loading sequence had no influence on the strength and deformational responses of the specimens. A horizontal crack at the base (just above the foundation) was visible before ultimate state in all the specimens. It was due to the sliding of the vertical reinforcement. It was observed from the literature that the sliding shear failure did not affect the force deformation characteristics of the wall. Pilakoutas and Elnashai (1995) tested six cantilever walls of aspect ratio 2 under severe cyclic loading up to failure. They found that shear reinforcement in excess with respect to the amount required to resist the maximum applied load did not affect the strength and deformational characteristics of the specimens. They demonstrated that the bulk of the energy dissipation of the shear wall is due to flexure. Recently, El-Azizy *et al*. (2015) tested walls of three different cross sectional configurations; rectangular, flanged and boundary elements with quasi-static displacement controlled cyclic loading. The seismic performance of the flanged wall type was found to be superior to that of their rectangular counterparts with respect to both the ultimate displacement capacity and ductility level. Carrillo *et al.* (2015) studied the effect of lightweight and low-strength concrete on seismic performance of thin lightly-reinforced shear walls and concluded that shear strength, drift ratios and energy dissipated at different limit states of lightweight concrete walls were larger in comparison to walls made of normal weight concrete. Though local ductility of each component (shear walls) is discussed in this paper, the global ductility of the structure will be different based on type of shear walls connected and also lateral load distribution which varies depending on configuration of structure. A general method for the analysis of the lateral loading distribution of three-dimensional structures composed of any kind of bracings is proposed by Carpinteri *et al*. in 2010 and detailed conceptual design of tall unconventionally shaped structures is discussed by Carpinteri *et al*. in 2014.

Shake table tests for shear walls have been carried out by few researchers (Coronelli *et al.* 2006, Matsui *et al.* 2004). A 1/3rd scale model (5.1 m tall) composed of two parallel five floor RC walls was tested in CEA France in CAMUS experiments by Coronelli *et al*. (2006), and it was concluded that shear-flexure coupling took place during the seismic tests and this phenomenon cannot be captured by monotonic tests. Dynamic shake table tests on two numbers of RCC shear walls were carried out by Matsui *et al*. (2004) and the test results were simulated by analysis. The envelope curve of the observed hysteresis relations with strength deterioration could be simulated

well up to shear failure by a macro model. Shaking table tests on two numbers of slender 8 storey RCC shear walls subjected to north American seismic ground motions have been carried out by Ghorbanirenanai *et al*. (2012). The response of these walls was significantly affected by the second mode, causing an inelastic flexural response observed at the base as well as at the sixth level. They also suggested that higher damping is expected in actual building structures compared with the test specimens and more research is demanded in this field. In 2012, Carrillo and Alcocer (2012) obtained the displacement and shear strength capacities, as well as the dynamic characteristics of six RC walls (solid walls and the walls with openings) under shaking table excitations. They observed that specimens with the walls openings exhibited a higher contribution of flexural deformations. Till date the behavior of cantilever lightly reinforced shear walls subjected to three different types of loads viz. static-monotonic, static-cyclic, and dynamic shake table test is seldom investigated. Besides this, it is necessary to carry out the accurate analytical simulation of these walls and evaluate of damping, stiffness reduction and performance limits for each type of loading. Hence in this paper, the behaviour of five numbers of mid-rise shear walls with aspect ratio 1.98 subjected to 3 different types of loads is studied. One wall was subjected to monotonic load, two walls were subjected to pseudo-static cyclic loads and two were subjected to earthquake loading using shake table experiments.

The analytical simulation of the experimental results is a very essential aspect and is performed by two types of modeling viz. micro and macro. Microscopic modeling approach which is based on a detailed interpretation of local behavior is used for simulation of monotonic and cyclic tests. Performing dynamic time history analysis using nonlinear concrete microscopic models require huge computational efforts and hence the main aim of the present work is to propose a simplified macroscopic model. In this work, the hysteretic macro-model, named the γ model, developed for RC walls by Lestuzzi and Badoux in 2003 is further modified by considering the stiffness degradation effect derived from the tests conducted. This modified model is then used for nonlinear dynamic analysis of shear walls. This model describes the experimentally observed stiffness degradation and the associated pinching of hysteretic loops. Finally ultimate load, drift limit, ductility and failure pattern of the walls are studied and variation of damping and stiffness values with drift are presented.

2. Details of the shear wall

The shear wall considered for the tests is 1:5 scaled model of internal structure of a nuclear power plant building. Schematic of Reactor building showing the shear wall is shown in Fig. 1(a).

The shear wall (7.8 m width, 15 m high and 1m thick) supports the steam generator of Indian type NPP and its first fundamental frequency is 3.1 Hz. This shear wall shows a cantilever type mode as the mass of steam generators is lumped at the top of the shear wall. 1: 5 scaled model of the shear wall with lumped mass on the top is obtained. Lumped mass on the top of the shear wall is obtained such that the frequency of the shear wall model along with lumped mass is 15.5 Hz as per scaling laws. The scaling and the design is based on the requirement that the shear wall shall reach ultimate strength and fail under seismic excitation within the capacity of shake table. Scaling laws are not used for acceleration given to the table and the time scale (frequency of time history). The shear wall with concrete (f'_c of 39 MPa) and steel (F_y of 415 Mpa) is designed as per Indian standard codes (IS 456 (2000), IS 13920 (2000)) for dead load and 0.4 g earthquake acceleration at the mass level of the wall. The model has 3 m height (h), 1.56 m width and 0.2 m thickness (t) and

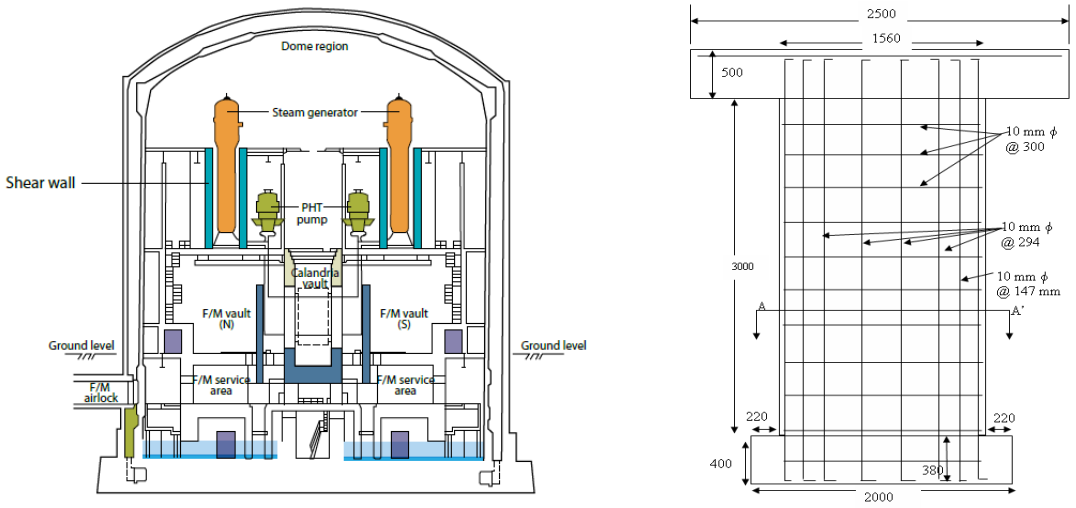

(a) Schematic of reactor building (b) Reinforcement details

Fig. 1 Shear wall details

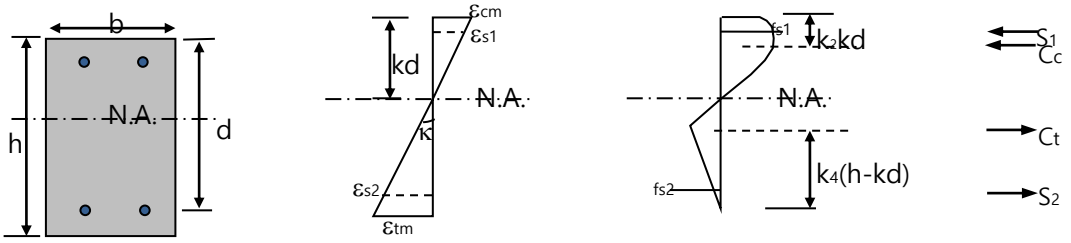

(a) Cross section (b) Stress strain relation

Fig. 2 Stress strain relation across concrete cross section

% age reinforcement of 0.4 % in vertical direction and 0.3 % in horizontal direction. The foundation is 0.4 m deep and 2 m×2 m in area and top slab is of dimensions 2.5 m×2.5 m×0.5 m. The reinforcement details of shear wall are given in Fig. 1(b). Mass of 8.5 tons in the form of concrete cube of dimension (1650 m×1650 m×1420 m) is added on the top slab and the mass of the top slab is 8 tons. Thus the shear walls will be subjected to total axial load of 16.5 tons and the axial load ratio is 0.03. Five numbers of such shear wall specimens are tested.

3. Theoretical study

3.1 Moment curvature relationship

The shear wall is a mid-rise shear wall with small axial compression and thus the failure of the shear wall is based on flexural yielding and the evaluation of flexural strength of the shear wall will be based on the basic principles. The design shear capacity of the shear wall is calculated from ACI code (2011) and is found to be 171 kN which is quite higher than the design flexural strength

of 90 kN. Mathematical model for the analysis of curvature and deflections of reinforced concrete shear wall in cracking stage is used.

In this model concrete will have a nonzero tensile capacity characterized by uniaxial stress strain diagram which undergoes strain softening due to progressive cracking. Linear crack opening law is assumed in which the stress strain relation in tension (Fig. 2(b)) follows a linear path with slope E_t after peak tensile stress f'_t has reached. E_t depends on the Young's modulus, *Ec* of concrete and the tensile strength of concrete f'_t. For concrete in uniaxial compression the stress strain relation covering compression softening (Fig. 2(b)) is used with Kent and Park (1971) model. Steel is assumed as elastic perfectly plastic. The normal force, *N* and moment, M equilibrium conditions for the shear wall using stress strain distribution across the section shown in Fig. 2(b), are written as follows

$$N = k_1 f_c^{'} bkd + \sum_{j=1}^{8} \sigma_{sj} A_{sj} - k_3 f_t^{'} b(h - kd) \tag{1}$$

$$M = k_1 f_c^{'} bkd\left(\frac{h}{2} - k_2 kd\right) + \sum_{j=1}^{8} \sigma_{sj} A_{sj}\left(\frac{h}{2} - d_i\right) + k_3 f_t^{'} b(h - kd)\left[\frac{h}{2} - k_4 (h - kd)\right] \tag{2}$$

Where parameter k_1 defines the average compressive stress and the resultant force acts at k_2kd below the compression face. Similarly k_3 denotes the resultant of tensile stress in concrete and the force acts at distance of k_4 (*h*-*kd*) from tension face.

The parameters k_1, k_2 and k_3, k_4 are described by expressions given below

$$k_1 = \frac{\int_0^{\varepsilon_{cm}} \sigma_c d\varepsilon_c}{f_c^{'} \varepsilon_{cm}}, \quad k_2 = 1 - \frac{\int_0^{\varepsilon_{cm}} \varepsilon_c \sigma_c d\varepsilon_c}{\varepsilon_{cm} \int_0^{\varepsilon_{cm}} \sigma_c d\varepsilon_c} \tag{3}$$

$$k_3 = \frac{\int_0^{\varepsilon_{tm}} \sigma_c d\varepsilon_c}{f_t^{'} \varepsilon_{tm}}, \quad k_4 = 1 - \frac{\int_0^{\varepsilon_{tm}} \varepsilon_c \sigma_c d\varepsilon_c}{\varepsilon_{tm} \int_0^{\varepsilon_{tm}} \sigma_c d\varepsilon_c} \tag{4}$$

The curvature of the shear wall at any moment capacity is given by

$$\kappa = \frac{\varepsilon_{cm}}{kd} \tag{5}$$

In order to calculate the moment curvature relation for a given axial load *N*, a succession of values of ε_{cm} increasing in small increments is considered and for each value of ε_{cm}, *kd* is obtained using Eq. (1). The curvature is then obtained from Eq. (5) and finally the moment for the particular value of curvature is obtained from Eq. (2). For the present shear wall (Fig. 3(a)), *b*=200 mm, *h*=1560 mm, A_{sj}= 157 mm^2 for *j*=1to 8, *d*=1520 mm, $f_c^{'}$=39.1 MPa, $f_t^{'}$=3.08 MPa, *Ec*=3.586×10^4 MPa, f_y=415 MPa, E_s=2×10^5 MPa. The moment curvature relation is obtained and force displacement relationship of the shear wall for monotonic increasing load is derived from it using principle of virtual work. Fig. 3(b) shows the load displacement relation for the shear wall, obtained from the moment curvature relation. The peak load is obtained as 195 kN.

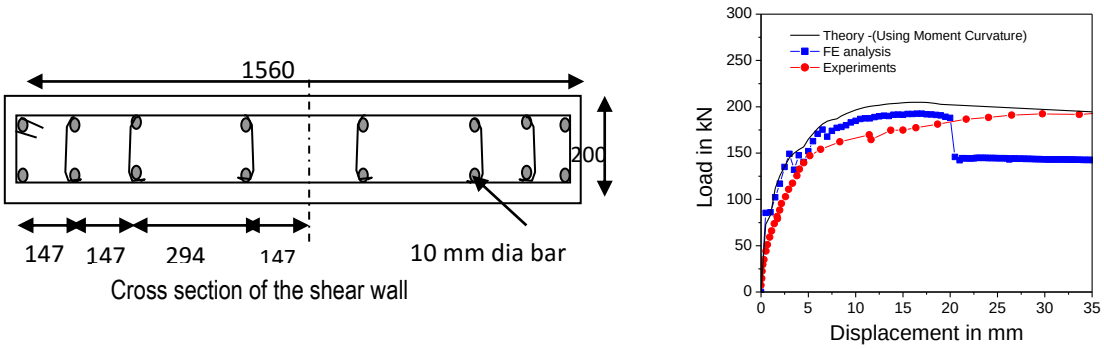

(a) c/s of Shear wall (b) Moment curvature relationship

Fig. 3 Shear wall moment curvature for the cross-section

Table 1

Shear Wall No.	Aspect ratio	Cube compressive strength (Mpa) 28 days	Yield stress of Rebars (MPa)	Loading Condition
SW1	1.92	46.1	437.67	Monotonic
SW2	1.92	45.2	423.56	Cyclic
SW3	1.92	46.7	419.52	Cyclic
SW4	1.92	46.5	410.56	Shake Table
SW5	1.92	45.4	429.85	Shake table

4. Experimental program

Five identical shear wall specimens (SW1-SW5) were considered for the tests. These were experimentally subjected to slow monotonic and cyclic horizontal loading regimes. Concrete used for all 5 specimens of shear walls was made from Portland cement, river sand and crushed gravel. Measured slumps ranged from 60 to 180 mm for all specimens. Compression tests were carried out on 6 numbers of 150×150 mm cubes for each shear wall. The details are mentioned in table1. The modulus of elasticity of concrete was calculated on the basis of data obtained from the cube compression tests. The concrete strain corresponding to its strength was measured for each specimen. Tension tests were carried out on 6 numbers of HYSD (High Yield Strength Deformed) reinforcement bars for each shear wall. The ultimate strength of rebars was in range of 545 MPa to 558 MPa. SW1 wall is subjected to monotonic increasing displacement controlled test till failure. SW2 and SW3 walls are subjected to pseudo static cyclic displacement controlled tests till failure and SW4 and SW5 are subjected to the same series of earthquake motions, the intensity of which were amplified gradually, until up to failure. The details of the test program is shown in Table 1.

4.1 Monotonic and cyclic tests

One specimen (SW1) was subjected to slow monotonic load to obtain the backbone load displacement curve. In order to simulate loading sequence that might be expected to occur during

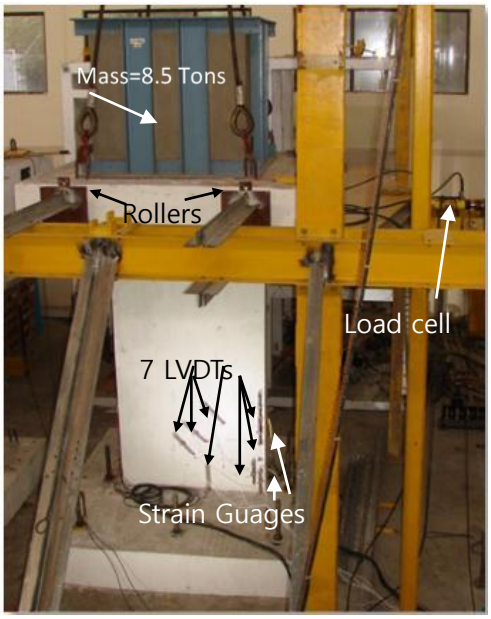

Fig. 4 Test set up (Monotonic and cyclic tests)

an earthquake, simplified type of horizontal cyclic loading history were adopted for other two wall specimens (SW2 and SW3). The test setup is shown in Fig. 4. The torsional mode of wall is prevented by supporting arrangement made for the top slab using rollers as shown in Fig. 4. The horizontal load was applied at a quasi-static rate in displacement controlled cycles with a hydraulic actuator having 500 KN capacity through a load cell. Displacement were applied in incremental fashion corresponding to three major states, namely cracking state, yielding state and ultimate state. Initially one cycle each of 0.4 mm, 2 mm and 4 mm peak displacement were given.

Then 3 cycles each of 6 mm, 8 mm, 10 mm,15 mm, 20 mm, 25 mm, 30 mm, 40 mm peak displacements were given in the loading programs. At each incremental loading state, the load was maintained constant for a few seconds in order to measure the data. The load, the displacement response of the walls and the steel strain via electronic data logger was measured and recorded. Strain gauges were used for measuring strains at 16 locations on vertical reinforcement as shown in Fig. 4. Extensometers (shown in Fig. 4) were used at 7 locations on surface of concrete for monitoring crack openings. Laser sensors were used in monitoring the in-plane horizontal displacements at top slab level (height 1560 mm above the foundation) of the wall. In order to ensure that the foundation is fixed to the laboratory's strong floor, vertical displacement of the top of the foundation was measured.

For the specimens SW1, SW2 and SW3, flexural cracks initially appeared near the bottom part of the tensile zone of the wall at cracking load of 80 kN and horizontal displacement of 0.44 mm. Yielding of the main reinforcement occurred at about 4 mm lateral displacement and strain in longitudinal reinforcement in the walls near bottom reached 2000 micro strain. The crack pattern at failure for the shear wall SW1 subjected to monotonic loads is shown in Fig. 5(a) and the load displacement curve obtained from test on SW1 is shown in Fig. 6(a). It is observed from Fig. 6(a) that the ultimate load for monotonic load (SW1 specimen) is 195 kN. For the same specimen the failure load is 142 kN and displacement at failure load is 62 mm. The other two shear wall

(a) Monotonic load (SW1) (b) Quasistatic cyclic load (SW2)

Fig. 5 Crack pattern in shear wall

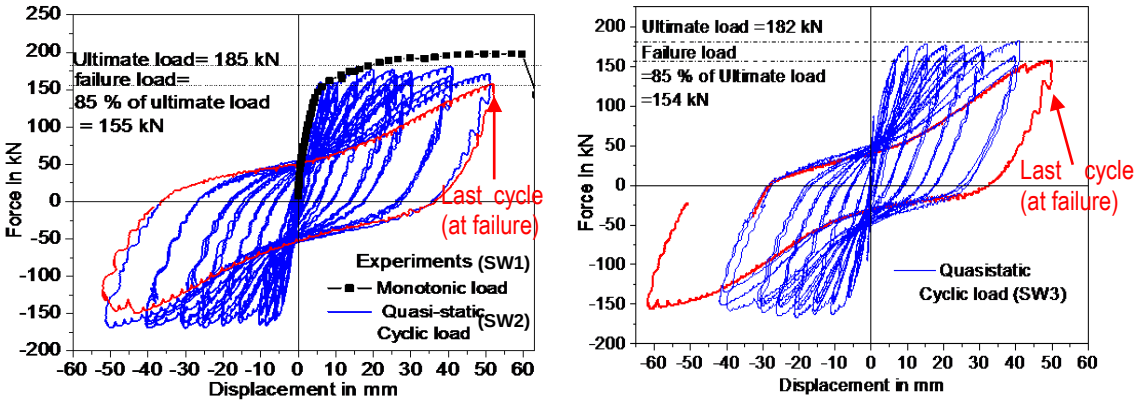

(a) Monotonic (SW1) and Cyclic tests (SW2) (b) Cyclic tests (SW3)

Fig. 6 Force displacement loop

specimens, SW2 and SW3 were subjected to cyclic loads with same loading protocol explained earlier. The load displacement curve obtained from experiments for SW2 and SW3 are shown in Fig. 6(a) and Fig. 6(b) respectively. For SW2 specimen (Fig. 6(a)), subjected to cyclic load ultimate load is 185 kN, failure load is 155 kN and the displacement at failure is 50 mm. In case of SW3 specimen as shown in Fig. 6(b) the ultimate load is 182 kN, failure load is 154 kN and the displacement at failure is 50 mm. For both the SW2 and SW3 specimens at the cyclic lateral displacement of about 6 mm flexural cracks progressed. As the lateral displacement approached 15 mm ultimate load was reached and significant inclined cracks were formed. Fig. 5(b) shows the crack pattern for shear wall specimen SW2. These cracks continued to penetrate deeply into the centre of the wall towards the compressive zone. It can be observed from Fig. 5(b) that these cracks formed a diagonally criss-crossing crack pattern for the specimen SW2 subjected to cyclic load. Similar crack pattern was observed for shear wall specimen SW3. At a lateral displacement of 40 mm, width of the major flexural cracks already developed increased. At this displacement which was just prior to failure, few semi-vertical cracks formed in the compressive zone and the concrete cover at lower compressive edge spalled off. This finally led to the failure of compressive zone of the wall at 50 mm lateral displacement.

Fig. 7 Crushing of concrete in the compression zone and buckling of main bars

Fig. 8 Test setup (Shake table tests)

The final failure of the wall occurred due to crushing of concrete in the compression zone of the wall and buckling of main reinforcement at the bottom between the two stirrups. This type of failure occurred at both the sides at the bottom corners. Fig. 7 illustrates the representative mode of failure of the walls which shows the buckling of the main reinforcement in between two stirrups.

4.2 Shake table tests

Two identical specimens, SW4 and SW5 were tested on shake table in the test setup as shown in Fig. 8. The out of plane deformation of the shear walls is restrained by setting steel frame as shown in Fig. 8. The steel frame was rigid with frequency of 40 Hz. The shake table was having capacity of 50 Tons with maximum acceleration of 1 g. Accelerometers and Laser displacement sensors were attached at the top slab and at the middle of shear wall to measure the acceleration and displacement of the shear wall at the top and middle. Initially sine sweep tests were carried out on the shear wall to evaluate the frequency and damping. Sine sweep excitation with peak of 0.04 g was given from 1 Hz to 43 Hz at constant sine sweep rate of 0.05 Hz per second for total time of 500 seconds. The input signal from 226 to 230 seconds is shown in Fig. 9(a). Output signal is shown in Fig. 9(b) from 0 to 280 seconds so that resonance is clearly visible. It is observed that resonance occurs at 230 seconds which gives a frequency of 11.5 Hz and the amplification factor for output to input is 7.7. Also some amplification is observed at 3.2 Hz at 60 seconds. The mass of 8.5 tons is attached to top slab through bolts. The fixity of the bolts to the top slab is not

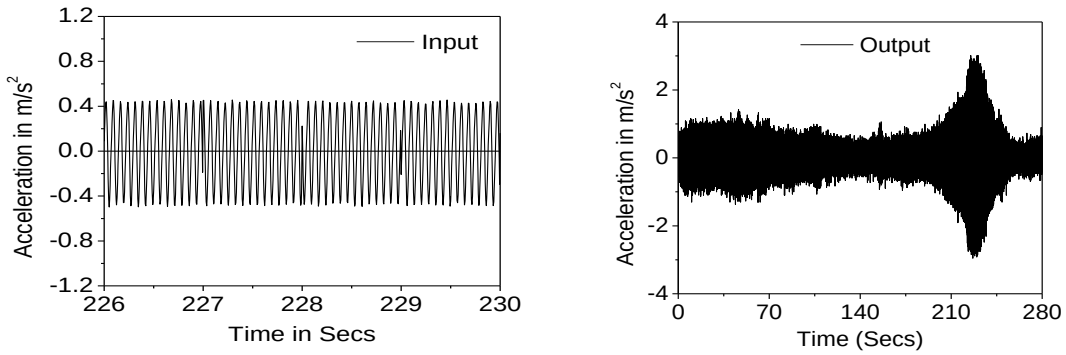

(a) Input (b) Output

Fig. 9 Transfer Function for shear wall

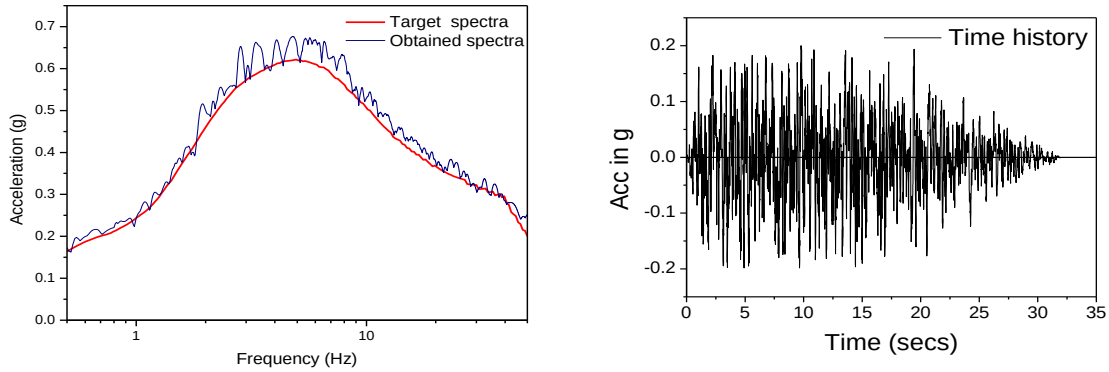

(a) Compatible and required spectrum (b) Time history

Fig. 10 Spectrum compatible time history

perfectly achieved and hence the top mass has a local frequency of 3 Hz which is the local mode of the mass. The global mode of the shear wall is 11.5 Hz. This wall has local frequency of 3.2 Hz which is the frequency of the mass attached to the top slab of the wall. Hence some amplification is observed at 3.2 Hz in the output signal. The wall frequency through analysis is obtained as 12 Hz. Damping ratio is obtained from the amplification of output to input signal at resonance and is found to be 0.06. The damping ratio for concrete shear walls as reported in literature (Chopra 2000) is 3 to 5 % for undamaged shear wall. However the value of 6% obtained from tests is slightly higher and can be accounted for friction between mass and top slab and the bolts. Two specimens of shear walls were subjected to same series of spectrum compatible time histories with increasing excitation from 0.1 g peak acceleration to 0.9 g peak acceleration. The input time history for 0.2 g peak acceleration and the compatible test spectrum along with required response spectrum is shown in Fig. 10.

At 0.5 g the strain in steel reached the yield strain of steel (about 1800 μm/m). The cracks formed in the shear wall (SW4) are shown in Fig. 11(a). Finally at 0.9 g PGA the walls failed due

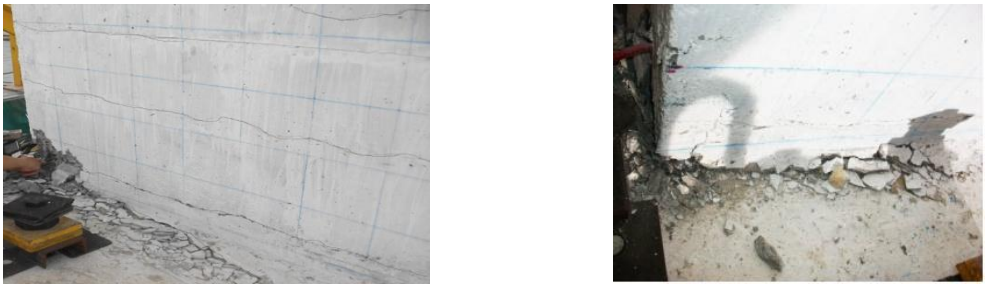

(a) Crack pattern in Shear wall (b) Final failure by sliding at base

Fig. 11 Failure in the shear wall in shake table tests

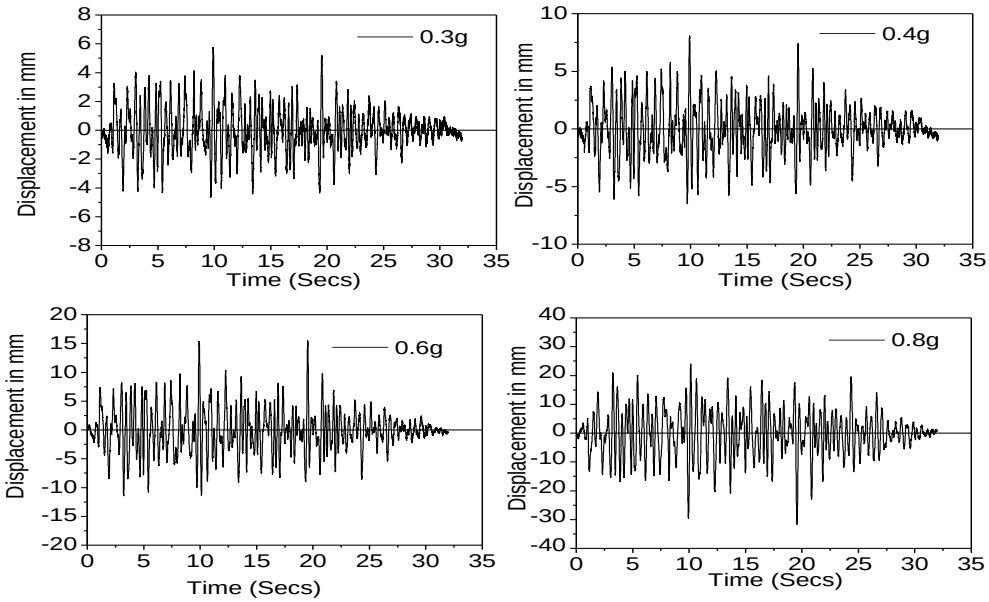

Fig. 12 Displacement time history relative to base for the shear wall from shake table tests

to sliding shear failure and the both the shear walls (SW4 and SW5) slide at the base (Fig. 11(b)). The relative displacement of the shear wall, SW4 with respect to base obtained from shake table tests for 0.3 g, 0.4 g, 0.6 g and 0.8 g peak base acceleration is shown in Fig. 12.

Total 9 runs were given to the shake table starting from 0.1 g to 0.9 g with increment of 0.1 g. At peak table acceleration of 0.2 g flexural cracks appeared in the bottom portion of shear walls. The flexural cracks propagated at the bottom part of the shear wall as the table base excitation increased. It is observed from Fig. 12 that the maximum displacement of the wall (SW4) before failure is 35 mm relative to base in the shake table test for excitation of 0.8 gPGA. Similarly for SW5 the relative displacement with respect to base at 0.8 g was observed to be 42 mm.

The acceleration obtained from the top mass is multiplied by the top mass value and the force taken by the mass is plotted with the relative displacement of the shear wall with respect to base.

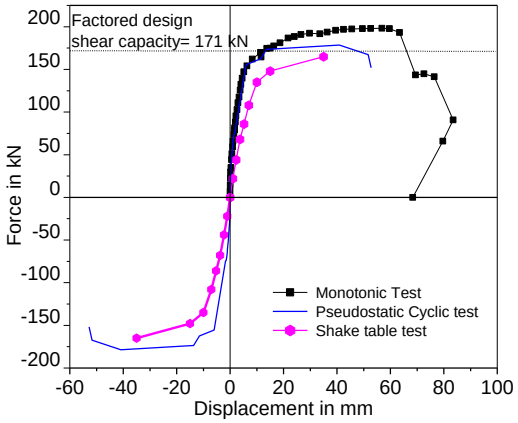

Fig. 13 Comparison of experimental F-δ diagram of the wall

The envelope of force displacement diagrams acquired from all the three tests is shown in Fig. 13. It is observed that the peak shear capacity obtained in Pseudo-static-cyclic tests and monotonic tests is higher than that obtained in shake table tests. The ductility and the ultimate drift of wall in static tests are also higher than that in shake table tests. This is due to repeated cycles of earthquake load given during the shake table tests due to which the stiffness is degraded by extensive cracking. The capacity the wall obtained from shake table tests is just equal to 171 kN.

5. Analytical simulation

5.1 Nonlinear analysis: static cyclic loading

Finite element analysis of RC shear wall is performed. 3D-RC shear wall slab structure is modeled using 4 noded iso-parametric 2D plane quadrilateral elements for wall and both top and bottom beams. Steel is modeled in discrete form of truss element for wall and smeared form in the top and bottom beams. Nonlinear concrete model is considered with a cylinder strength of 39 MPa (Considering cube strength 46 Mpa). Kent and Park (1971) concrete material model is chosen for the analysis which includes non-linear behavior in compression including hardening and softening. Fracture of concrete in tension is based on the nonlinear fracture mechanics. The biaxial strength failure criterion (Kupfer 1969), reduction of compressive strength after cracking, tension stiffening effect and reduction of the shear stiffness after cracking is also considered in the model. The reduction of compressive strength after cracking shown by factor β is considered as 0.8. The steel is modeled as reinforcement bars with a bilinear elastic-plastic model with a yielding strength of 415 MPa. The boundary conditions during the experiments are simulated in the analysis as accurately as possible. The horizontal and vertical displacement at the base of the wall is assumed to be zero in the FE model. The vertical translational degree of freedom at top slab is free and horizontal displacements are applied at that node of top slab in incremental manner. The vertical load of 8.5 tons is applied uniformly on the top slab. The crack band theory is used in the analysis for accurate determination of cracks. Analysis is carried out for monotonic loading and pseudo-static cyclic loading. The loading protocol for the analysis is the same as given in tests for cyclic

loads. Fig. 14(a) shows the crack pattern in the wall at failure obtained from analysis. It is observed from the figure that failure of the shear wall is due to bending loads and flexural cracks are seen in the FE model. The load deflection relationship for monotonic loading and cyclic load obtained from analysis is shown in Fig. 14(b). It is observed that the monotonic load deflection characteristics envelopes the cyclic characteristics. It is observed from analysis that the loads corresponding to performance states of first cracking, yielding of reinforcement and ultimate state are 75 kN, 140 kN and 185 kN respectively. The deflections at cracking and yielding obtained from analysis are 0.45mm and 4 mm respectively. The displacement at failure load from analysis is 25 mm. The displacement ductility of the wall which is the capacity of the wall to deform beyond its elastic limit is obtained as 6 from the analysis. The force displacement curve obtained from FE analysis (Fig. 14(b)) is in good agreement with that obtained from experiments (Fig. 6). However the instabilities, such as rebar buckling and rebar fracture are typically not considered in models. Hence the exact failure displacement of the wall obtained in experiments is not captured in analysis.

5.2 Nonlinear dynamic analysis

Evaluation of the shear wall subjected to earthquake loading needs detailed nonlinear dynamic analysis of shear wall subjected to spectrum compatible time history. Nonlinear dynamic analysis using micro-modeling will require large computational efforts and hence the most efficient and reliable modeling for this type of analysis is by using macro-models. The shear wall undergoing seismic excitation is thus modeled as non-linear single-degree-of-freedom (SDOF) system using a multi-linear hysteretic model. Earlier several attempts were made by researchers (Takeda *et al*. 1970, Saiidi and Sozen 1979, Ozcebe and Saatcioglu 1989, Al-Sulaimani and Roessett 1985) to develop a model of the hysteretic behavior of shear wall. The models developed by the above researchers are quite complex though they considered stiffness degradation of concrete during reloading and unloading. Moreover, these models require high computational efforts. Lestuzzi and Badoux (2003) developed a simple multi-linear model of shear wall which was robust and computationally efficient as well as no numerical instability was observed in the model. However this model did not consider the stiffness degradation of the shear wall. Hence, the simple multi-linear model developed by Lestuzzi and Badoux (2003) is further modified by considering stiffness degradation effect using the parameters obtained from the present experiments.

5.2.1 Multilinear model

Non-linear SDOF system is defined by the force-displacement relationships of hysteretic model using six parameters: the initial stiffness (stiffness before cracking), yield stiffness, the yield displacement, the post yield stiffness, stiffness degradation depending on ductility and the value of γ which represents pinching effect. The initial stiffness, yield displacement, yield stiffness and the post yield stiffness of the model are taken as per load displacement curve obtained from monotonic tests and cyclic tests (Fig. 6(a)). Thus the initial stiffness before cracking is 166.7 kN/mm, yield displacement is 4 mm, yield stiffness is 35 kN/mm and post yield stiffness is 1.28 kN/mm. The force displacement hysteretic rule is explained for the multi-linear model as shown in Fig. 15(a). The comparison of multi-linear model with cyclic tests is shown in the Fig. 15(b). The constitution of model is based on the observation that the reloading and the unloading curves tend to cross at the same point on the elastic portion of the curve. The force-displacement relationships of the Elasto-plastic model are modified in such a way that the reloading curves of large yield

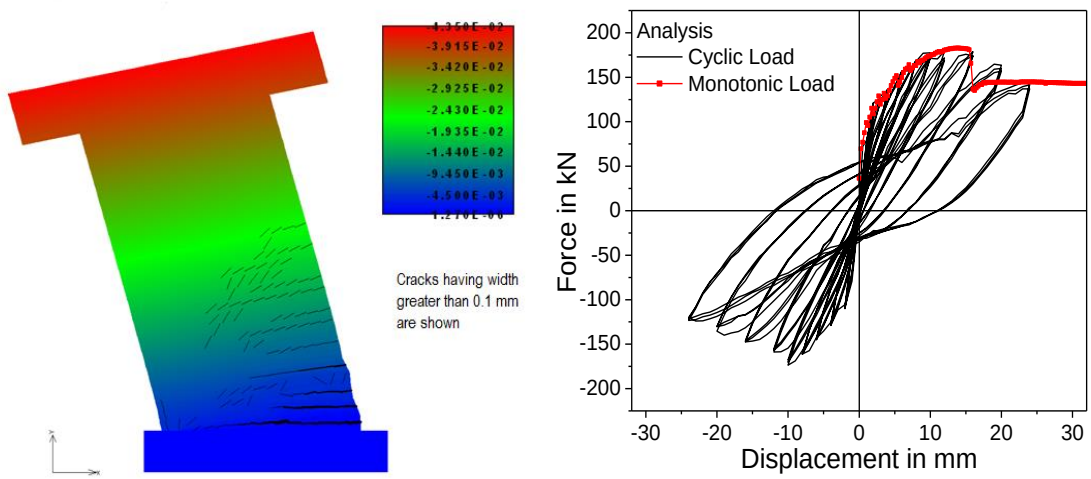

(a) Deflected shape and crack pattern at Failure (b) Comparison of test and analysis hysteresis

Fig. 14 Analysis results of the shear wall

excursions cross the elastic portion of the envelope at a height of 1-γ of the yield force. If the peak displacement is lesser than the maximum displacement (δ_{max}) then the reloading curves aim to the current peak displacement. It is observed from Fig. 15(b) showing cyclic test hysteresis, that the point at which reloading curves tend to cross is obtained as 60.7 kN and the same is adopted in the model. Thus the factor γ derived from the experiments is 0.55. Moreover, the comparison of multi-linear model hysteretic curves with cyclic tests (Fig. 15(b)) at various ductility shows that the unloading stiffness/ reloading stiffness is reduced and is lesser than the initial stiffness of the wall. The ratio of yield stiffness to initial stiffness (stiffness before cracking) is obtained as 0.21 for the wall. This reduction in stiffness represent the damage occurred in the shear wall and the stiffness goes on decreasing with increase in excitation and the corresponding damage. The stiffness degradation factor, c which is the ratio of reduced stiffness to the initial stiffness is plotted with ductility (Fig. 16). At ductility 1 the stiffness degrading factor c is thus 0.21 and the stiffness degradation in the unloading/reloading stiffness is about 0.06 at the failure of wall specimen. The parameter c is given by the relation given as per Eq. (6)

$$c = 0.06 + 0.21e^{-\mu/2.75} \tag{6}$$

Where μ is the ductility. The unloading/ reloading stiffness at various levels of deformation can be obtained as K_2, K_3 etc. If the peak displacement of any cycle is less than the maximum displacement occurred during the loading then the unloading/reloading stiffness will remain the same as the unloading stiffness of the maximum displacement hysteretic loop. This can be explained from Fig. 15(a) showing load deformation hysteretic path OABCDEF-FGHIJML. It can be inferred from the Fig. 15(a) that $K_3<K_2<K_1$ and $K_4=K_3$. Similarly it is seen that $K'_2<K'_1$ and $K'_3=K'_2$. When unloading occurs at any nth level of displacement greater than or equal to yield displacement, the stiffness can be given as

$$K_n = c\, K_i \tag{7}$$

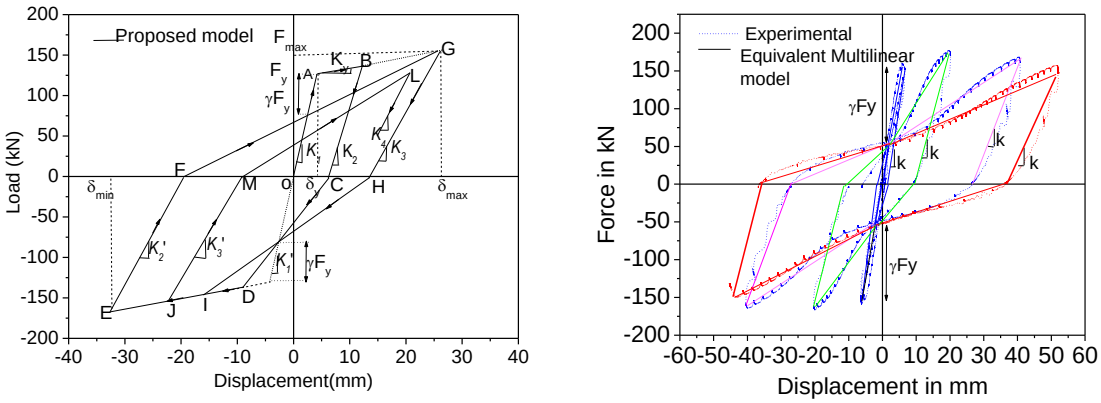

(a) Multi-linear (b) Comparison of experimental and analytical

Fig. 15 Hysteretic model

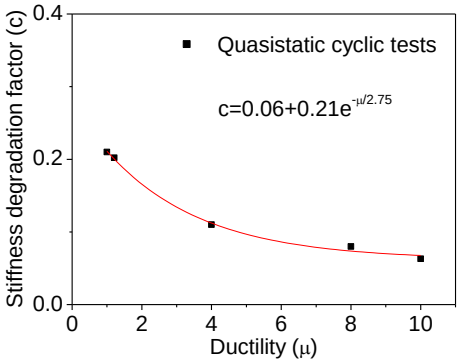

Fig. 16 Relation of stiffness degradation with displacement ductility

Where c is obtained from Eq. (6) corresponding to the displacement ductility achieved at the peak displacement of that loop and K_i is the initial stiffness (stiffness before cracking of the shear wall).

The force deformation relations on the paths in Fig. 15(a) are as follows

Elastic (loading), Path O-A

$$F(t) = K_1 x(t) \tag{8}$$

Post yield deformation (loading), Path A-B and Path D-E (replace F_y, δ_y by $-F_y$, $-\delta_y$)

$$F(t) = F_y + K_y(x(t) - \delta_y) \tag{9}$$

Elastic with stiffness degradation (unloading),

Path B-C where displacement and force at B is x_m and F_m and Path E-F where displacement and force at E is x_l and F_l (replace F_m, x_m by F_l, x_l)

$$F(t) = F_m + K_2(x(t) - x_m) \tag{10}$$

Where, K_2 is obtained from Eq. (7) and value of c from Eq. (6) at ductility value of x_m/x_y

The unloading and reloading curve at large yield excursions cross elastic portion of envelope at height (1-γ) of the yield force. Considering displacement at C is x_c and displacement at F is x_f,

Path C-D and Path F-G,

$$F(t)=[(1-\gamma)\, F_y/(\delta_y(1-\gamma)+x_c)] \times (x(t)-x_c) \tag{11}$$

For reloading curve (path M-L) when peak displacement (displacement at point J) of the loop is lesser than the maximum displacement (displacement at point E) then the reloading curves aim to the current peak displacement and thus $F(t)$ can be obtained.

5.2.2 Hysteretic damping

The hysteretic damping is a very important parameter and is essentially used to evaluate accurate response of structures deforming in the nonlinear range. Response of reinforced concrete structures deforming in nonlinear range can be evaluated by linearization techniques using linear analysis with equivalent reduced stiffness and hysteretic damping. The nonlinear behavior is also to be represented by equivalent viscous damping factor, ζ_{eq} consisting of elastic and hysteretic energy dissipation. The equivalent viscous damping is divided into two parts as given by the equation given below.

$$\zeta_{eq} = \zeta_0 + \zeta_{hyst} \tag{12}$$

Where ζ_0 corresponds to initial damping in the elastic range and ζ_{hyst} corresponds to equivalent viscous damping ratio that represents energy dissipation due to nonlinear hysteretic behavior. Based on the work of Jacobsen (1930), the equivalent hysteretic damping is given by the equation

$$\zeta_{hyst} = (1/4\pi)\frac{Eh}{Es} \tag{13}$$

Where, Eh is the hysteretic energy dissipated by the structure and Es is the strain energy stored by the structure. Accurate evaluation of hysteretic energy is needed in order to obtain realistic equivalent damping of the nonlinear structure. The hysteretic energy can be obtained by evaluating the exact area of force displacement curve of the yielding concrete structure taking into consideration the stiffness degradation, pinching and strength degradation. Response analysis under earthquake excitations reveals that both the maximum displacements and the number of large-amplitude displacement response cycles increase significantly with the reduction in energy dissipation capacity, resulting in higher damage. Damage is defined as the deterioration in the effective stiffness of a displacement cycle, which is in turn related to the reduction in the energy dissipation capacity. Sucuoglu and Erberick (2004) carried out of cyclic tests on beams and gave an energy based hysteretic model which has strength reduction at a current displacement cycle by evaluating the loss in the energy dissipation capacity along the completed displacement path. This reduced energy dissipation can be implicitly accounted by pinching effect. The area of first and the damaged hysteretic loop shown in Fig. 17 can be calculated by the equations given below which takes into account stiffness and strength degradation.

$$E_{h1} = 2.5\, F_y\, (\delta_m - \delta_y) \tag{14}$$

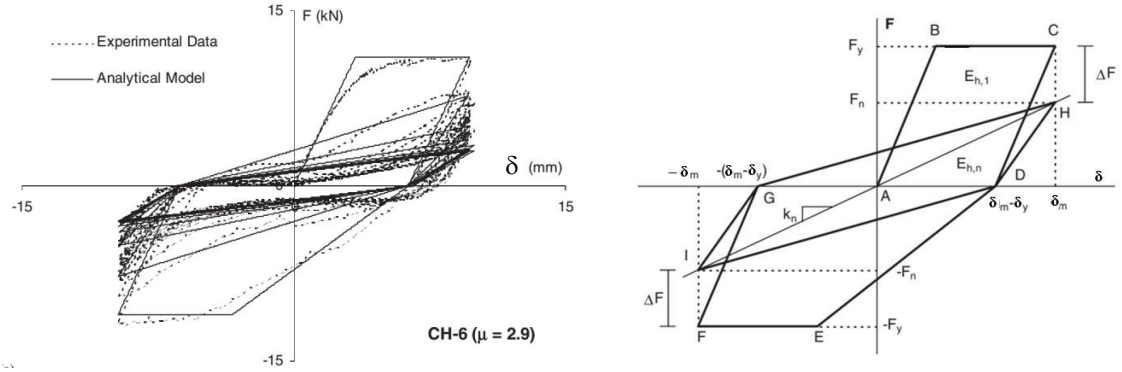

(a) Experiments (Sucuoglu and Erberick (2004)) (b) Schematic Force displacement loop

Fig. 17 Stiffness and strength degradation in cyclic force-deformation curve

$$E_{hn} = 2 F_n (\delta_m - \delta_y) \tag{15}$$

Where, F_y = Yield force, δ_m = ultimate displacement, δ_y = Yield displacement, F_n is the reduced strength after n cycles. From fatigue model described by Erberick and Sucuoglu (2004), F_n= 0.25 F_y for more than four cycles. The average hysteresis energy per cycle considering first and last cycle is given by the expression

$$E_{havg} = 0.5 * (2.5 + 2 \times 0.25) \{F_y(\delta_m - \delta_y)\} = 1.5F_y(\delta_m - \delta_y) \tag{16}$$

Strain energy per cycle is given as follows

$$E_0 = 0.5 \times Fy \times \delta_m \tag{17}$$

$$\xi = \frac{1}{4\pi} \frac{1.5 \times F_y \times (\delta_m - \delta_y)}{0.5 \times F_y \delta_m} \tag{18}$$

Considering, $\mu = \delta_m/\delta_y$

$$\xi_{HE} = \frac{1}{\pi} \times 0.75 \times \frac{(\mu - 1)}{\mu} \tag{19}$$

For concrete walls Priestley and Grant (2005) has given the hysteretic damping ratio as

$$\xi_{HE} = \frac{0.95}{\pi} \times (1 - \frac{1}{\sqrt{\mu}}) \tag{20}$$

The peak displacements of the wall are obtained from shake table tests at each peak base excitation for 0.1 g to 0.8 g as shown in Fig. 13. Using these peak displacements, at each base excitation level, ductility values are obtained considering yield displacement of the wall as 4 mm. The plot of ductility of wall for each base excitation is shown in Fig. 18(a). Damping ratio is obtained by Eq. (12) considering hysteretic damping as per Eq. (19) for various peak base excitation and is thus plotted using the respective ductility value as shown in Fig. 18(a). The damping ratio is in good agreement with that given by Priestley and Grant (2005) as shown in the same figure.

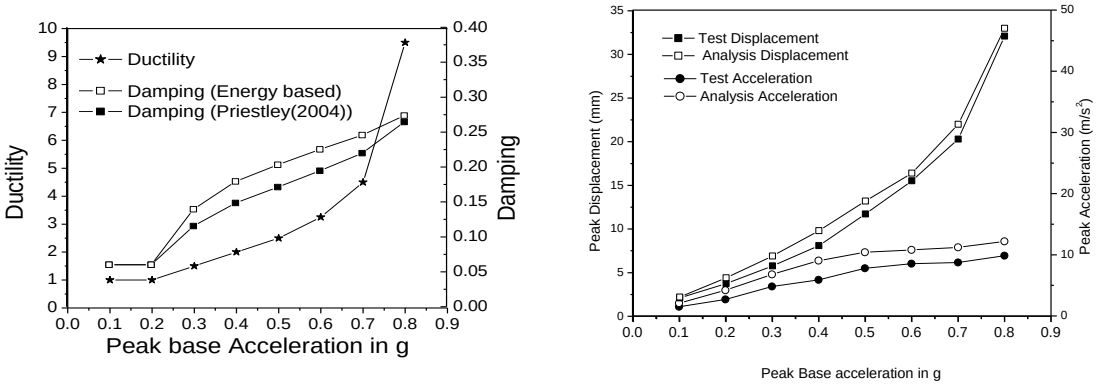

(a) Ductility and Damping ratio (b) Experimental and analytical peak responses

Fig. 18 Variation with peak base excitation

Post test nonlinear dynamic analysis of shear wall is carried out considering it as a SDOF system hysteretic model, explained above and mass of 16500 kg lumped at the top of shear wall. Analysis is carried out for the spectrum compatible time histories with PGA 0.1 g to 0.8 g with increment of 0.1 g. The damage occurred in the concrete wall due to previous time history excitation for each level of earthquake is considered in the analysis by reducing the initial stiffness of the wall and increasing the damping level for each excitation. The damping value taken into consideration for analysis for particular excitation is the damping obtained from Fig. 18(a) for previous excitation. Analysis is carried out using Wilson-theta method with θ=1.4 for the time increment of 0.0005 sec. The comparison of experimental (shake table tests) peak displacements and accelerations with analytically obtained values at each peak base excitation are shown in Fig. 18(b).

It is observed that peak displacements from analysis and experiments are in good agreement with each other. In the shake experiments, relative displacements and accelerations were measured at each time step however load cell was not attached to the top slab or mass. Hence hysteretic force displacement was not measured. Only the displacement and acceleration time histories measured from shake table tests were compared with analysis. The comparison of displacement and acceleration time histories of the top of the shear wall obtained from tests and analysis is shown in Fig. 19(a) and Fig. 19(b) for 0.5 g and 0.7 g, peak base acceleration respectively. Relative displacement time history was obtained from table displacements and the laser sensors attached to the top slab. It is observed that the analytical and experimental time history responses are in good agreement with each other. Analysis for 0.5 g peak base excitation is carried out using hysteretic model described earlier, by considering stiffness reduction and damping of 0.4 g peak base excitation. At 0.4 g, ductility of wall is 2 as shown in Fig. 18(a) and damping is 12%. Hence, considering initial stiffness in hysteretic model as given by Fig. 16 for ductility 2 and 12% damping nonlinear time history analysis is carried out for 0.5 g peak base excitation. Similarly analysis is carried out for 0.7 g peak base excitation. The analytical force displacement characteristics of the of the shear wall for 0.5 g and 0.7 g peak acceleration are shown in Fig. 20. It is observed that at 0.5 g the hysteretic deformation is less than at 0.7 g. The multi-linear hysteretic relation shown in Fig. 20 predicts the test displacement accurately for 0.5 g and 0.7 g peak base excitation level.

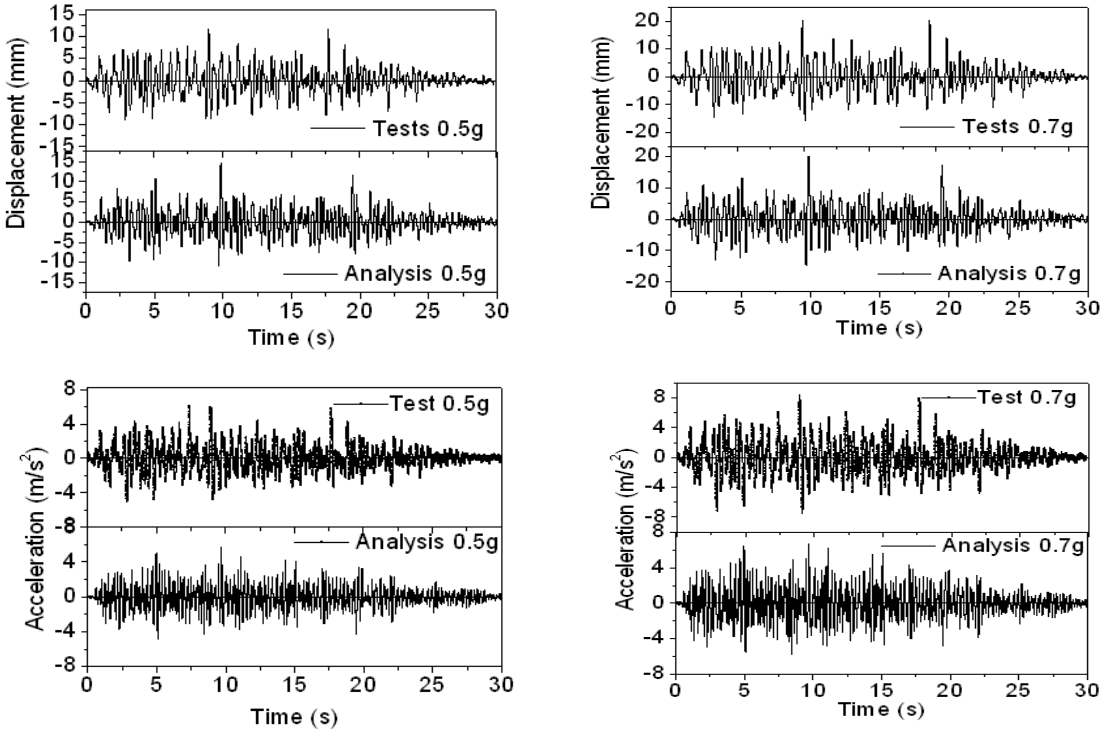

(a) 0.5 g peak base acceleration (b) 0.7 g peak base acceleration

Fig. 19 Comparison of test and analysis response of shear wall

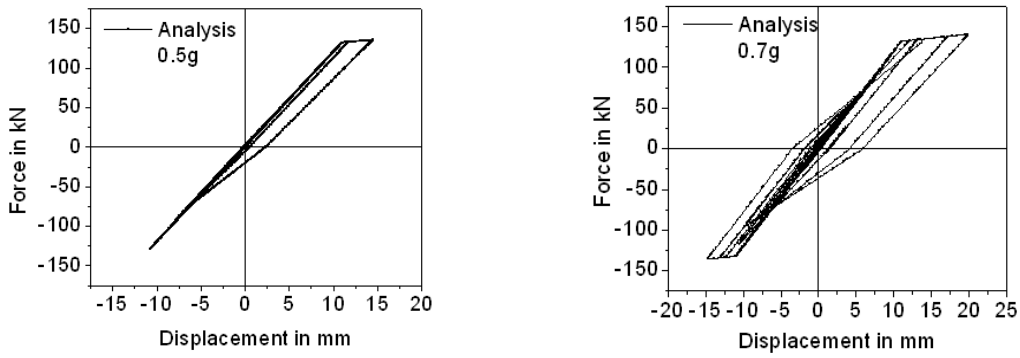

(a) 0.5 g peak base excitation (b) 0.7 g peak base excitation

Fig. 20 Force displacement characteristics

It is observed that the damage occurring to the wall at 0.7 g is higher than 0.5 g and thus the energy dissipation will be higher. It is observed from Fig. 18(a) that the total damping at 0.8 g comprising of elastic damping and damping due to hysteresis deformation of concrete is about 25%. Hence maximum hysteretic equivalent damping of about 20% is provided by the reinforced

concrete shear wall of aspect ratio 2 at failure. This damping is due to both stiffness and strength degradation occurring in the RC shear wall for repeated higher excitation levels of shake table. However, in Nuclear power plants RCC structures, the maximum level of earthquake considered in design is Safe Shutdown Earthquake (SSE). SSE earthquake level peak ground acceleration considered for the design is 0.2 g. The damping considered in design of RCC structures for SSE level is 7% which is in good agreement with Fig. 18(a) where it is observed that for 7% damping PGA is 0.22 g.

6. Conclusions

The crack patterns and failure mode of all the shear walls indicate that the wall capacity is affected by the flexural as well as shear strength of the specimen. For the two walls specimens with cyclic loading, the plastic hinge was formed at the extreme fibre of the wall section and at the vicinity of the base. A horizontal crack is observed at the base (just above the foundation) prior to ultimate state, may be due to sliding of the vertical reinforcement. The force displacement relation obtained from analysis for pseudo-static cyclic loading predicts the test accurately up to a horizontal deflection of 25 mm. From the quasi-static cyclic experiments, the ultimate load is obtained as 185 kN and ultimate drift is obtained as 1.6% which is more than the drift for collapse prevention performance level of 0.75% stated in FEMA-356. The drift obtained is in good agreement with that mentioned by Duffey *et al*. (1993) for the wall with aspect ratio of 2. Parallel flexural cracks were developed below the mid height of the wall and final failure of the walls occurred due to sliding shear failure for the two shear wall specimens subjected to shake table tests. Thus it is observed that though sliding shear failure was observed in the walls it did not affect the force deformation characteristics of the wall. This was also reported by as reported Pilakoutas and Elnashai (1995) for cyclic tests. The ultimate load and displacements obtained from shake table tests are lower than that obtained from pseudo-static cyclic tests. This is because the wall is subjected to more number of cycles in shake table tests than the quasi-static cyclic tests hence it has undergone more deterioration. The nonlinear dynamic response obtained from shake table tests can be well predicted by performing dynamic analysis using proposed multi-linear stiffness degrading macro-model. The maximum hysteritic damping obtained from the wall due to cracking at the collapse of the wall is 20%. Evaluation of equivalent stiffness and damping can be useful for designers to predict the nonlinear response of the slender shear walls using linearization techniques.

References

ACI-318 RM-89 (2011), *Building code requirements for reinforced concrete*, American Concrete Institute-318.

Al-Sulaimani, G.J. and Roessett, J.M. (1985), "Design spectra for degrading system", *ASCE J. Struct. Eng.*, **111**(12), 2611-2623.

Carpinteri, A., Corrado, M., Lacidogna, G. and Cammarano, S. (2012), "Lateral load effects on tall shear wall structures of different height", *Struct. Eng. Mech.*, **41**(3), 313-337.

Carpinteri, A., Lacidogna, G. and Cammarano, S. (2014), "Conceptual design of tall and unconventionally shaped structures: a handy analytical method", *Adv. Struct. Eng*., **17**, 767-783.

Carpinteri, A., Lacidogna, G. Puzzi, S. (2010), "A global approach for three-dimensional analysis of tall

buildings", *Struct. Des. Tall Spec. Build*., **19**, 518-536.
Carrillo, J. and Alcocer, S.M. (2012), "Seismic performance of concrete walls for housing subjected to shaking table excitations", *Eng. Struct*., **41**, 98-107.
Carrillo, J., Lizarazo, J.M. and Bonett, R. (2015), "Effect of lightweight and low-strength concrete on seismic performance of thin lightly-reinforced shear walls", *Eng. Struct*., **93**, 61-69.
Chopra, A.K. (2000), *Dynamics of Structures: Theory and Application to Earthquake Engineering*, Prentice Hall, New Jersey.
Coronelli, D., Martinelli, L., Martinelli, P. and Mulas, M.G. (2006), "Micro-Meso-Macro scale modelling and analysis of the camus I", *First European Conference on Earthquake Engineering and Seismology*, Paper No. 1478.
Duffey, T.A., Goldman, A. and Farrar, C.R. (1993), "Shear wall ultimate drift limits", USNRC, NUREG/CR-610.
El-Azizy, O.A., Shedid, M.T., El-Dakhakhni, W.W. and Drysdale, R.G. (2015), "Experimental evaluation of the seismic performance of reinforced concrete structural walls with different end configurations", *Eng. Struct*., **101**, 246-263.
FEMA-356 (2000), Prestandard and Commentary for the Seismic Rehabilitation of Buildings.
Ghorbanirenan, I., Tremblay, R., Léger, P. and Martin, L. (2012), "Shake table testing of slender RC shear walls subjected to Eastern North America seismic ground motions", *J. Struct. Eng.*, ASCE, **138**, 1515-1529.
IS 13920,(1993) Indian Standard, Ductile detailing of reinforced Concrete structures subjected to seismic forces-code of practice, India
IS 456, (2000) Indian Standard, Plain and reinforced concrete- code of practice, Fourth Revision., India
Jacobsen, LS. (1930), "Steady forced vibrations as influenced by damping", *ASME Tran.*, **52**, 169-81.
Kassem, W. (2015), "Shear strength of squat walls: a strut-and-tie model and closed-form design formula", *Eng. Struct*., **84**, 430-438.
Kent, D.C. and Park, R. (1971), "Flexural mechanics with confined concrete", *J. Struct. Div.*, ASCE, **97**(7), 1969-1990.
Kupfer, H., Hilsdorf, H.K. and Rusch, H. (1969), "Behavior of concrete under biaxial stresses", *ACI J.*, **66**, 656-666.
Lestuzzi, P. and Badoux, M. (2003), "The gamma-model: a simple hysteretic model for reinforced concrete", *Proceedings of the Fib-Symposium, Concrete Structures in Seismic Regions*, Athens, Greece.
Matsui, T., Kabeyasawa, T., Koto, A., Kuramoto, T. and Nagashima, I. (2004), "Shaking table test and analysis of reinforced concrete walls", *13th World Conference on Earthquake Engineering*, Canada, Paper No. 419.
Ozcebe, G. and Saatcioglu, M. (1989), "Hysteretic shear model for reinforced concrete members", *ASCE J. Struct. Eng.*, **115**(1), 132-148.
Paulay, T., Priestley, M.J.N. and Synge, A.J. (1982), "Ductility in earthquake resisting squat shear walls", *ACI J. Proceed.*, **79**(4) 257-269.
Pilakoutas, K. and Elnashai, A.S. (1995), "Cyclic behaviour of RC cantilever walls, Part I: experimental results", *ACI Struct. J*., **92**(3), 271-281.
Priestley, M.J.N. and Grant, D.N. (2005), "Viscous damping for analysis and design", *J. Earthq. Eng.*, **9**(spec02), 229-255.
Saiidi, M. and Sozen, M.A. (1979), "Simple and complex models for nonlinear seismic response of reinforced concrete structures", Technical Report Research Series No. 465, University of Illinois, Urbana, USA.
Salonikios, T.N. (2002), "Shear strength and deformation patterns of R/Cwalls with aspect Ratio 1.0 and 1.5 designed to Eurocode8 (EC8)", *Eng. Struct*., **24**, 39-49.
Sucuoglu, H. and Erberik, A. (2004), "Energy based Hysterisis and damage models for deteriorating systems", *Earthq. Eng. Struct. Dyn.*, **33**,69-88.
Takeda, T., Sozen, M.A. and Nielsen, N.N. (1973), "Reinforced concrete response to simulated earthquake", *ASCE J. Struct. Div*., **96**(12), 2557-2573.

Tasnimi, A.A. (2000), "Strength and deformation of mid-rise shear walls under load Reversal", *Eng. Struct.*, **22**, 311- 322.

CC